

## Non-invasive and quantitative near-infrared haemoglobin spectrometry in the piglet brain during hypoxic stress, using a frequency-domain multidistance instrument†

D M Hueber<sup>1</sup>, M A Franceschini<sup>2</sup>, H Y Ma<sup>3</sup>, Q Zhang<sup>3,4</sup>,  
J R Ballesteros<sup>5</sup>, S Fantini<sup>2</sup>, D Wallace<sup>1</sup>, V Ntziachristos<sup>6</sup> and B Chance<sup>3</sup>

<sup>1</sup> ISS Inc., 1602 Newton Drive, Champaign IL 61822, USA

<sup>2</sup> Bioengineering Center, Department of Electrical Engineering and Computer Science, Tufts University, 4 Colby Street, Medford, MA 02155, USA

<sup>3</sup> School of Medicine, Johnson Research Foundation, Department of Biochemistry and Biophysics, University of Pennsylvania, D501 Richards Building, Philadelphia, PA 19104, USA

<sup>4</sup> NMR Center, MGH Building 149, 13th Street, Rm2301, Charlestown, MA 02129, USA

<sup>5</sup> St. Christopher's Hospital for Children, Department of Neonatology,

Erie Avenue at Front Street, Philadelphia, PA 19134, USA

<sup>6</sup> Department of Pediatrics, Medical College of Pennsylvania, Philadelphia, PA 19104, USA

Received 2 May 2000, in final form 12 September 2000

### Abstract

The frequency-domain multiple-distance (FDMD) method is capable of measuring the absolute absorption and reduced scattering coefficients of optically turbid media. Absolute measurement of absorption at two near-infrared (NIR) wavelengths makes possible the quantitation of tissue haemoglobin concentration and tissue haemoglobin oxygen-saturation (StO<sub>2</sub>). However, errors are introduced by the uncertainties of background absorption and the dissimilarities between real tissues and the simplified mathematical model on which these measurements are based. An FDMD-based tissue instrument has been used for the monitoring of tissue haemoglobin concentration and oxygenation in the brain of newborn piglets during periods of hypoxia and hyperoxia. These tissue haemoglobin saturation values were compared with arterial saturation (SaO<sub>2</sub>) and venous saturation (SvO<sub>2</sub>) measured by blood gas analyses. A linear correlation was observed between StO<sub>2</sub> and the average of SaO<sub>2</sub> and SvO<sub>2</sub>. However, StO<sub>2</sub> is not equal to any fixed weighted average of SaO<sub>2</sub> and SvO<sub>2</sub> unless we introduce an effective background tissue absorption. The magnitude of the background absorption was about 0.08 cm<sup>-1</sup> at 758 nm and 0.06 cm<sup>-1</sup> at 830 nm, and it was nearly consistent between piglets. The origin of this 'effective' background absorption may be real, an artefact caused by the application of a simplified model to a complex sample, or a combination of factors.

† This work was carried out at the University of Pennsylvania, School of Medicine in Philadelphia, Pennsylvania.

## 1. Introduction

Because light in the wavelength range 700–900 nm can penetrate several centimetres into many tissues, it has been used for the non-invasive determination of absorbing species in living tissue, especially haemoglobin (Jöbsis 1989, Chance 1989, Wahr *et al* 1996, Chance and Alfano 1997, Chance *et al* 1999). However, early use of ‘quantitative’ near-infrared spectroscopy (NIRS) was limited because it is not accurate to simply apply the Beer–Lambert law in optically turbid media. Developments in NIRS have attacked this problem, including the use of time-resolved spectroscopy and the corresponding development of theoretical models that describe light propagation in highly scattering media (Chance 1989, Arridge *et al* 1992, Benaron *et al* 1989, Patterson *et al* 1989, Karagiannes *et al* 1989, Farrel *et al* 1992, Cope *et al* 1991, Benaron and Stevenson 1993, Miwa *et al* 1995, Sevick *et al* 1991, Cope and Delpy 1988, Tromberg *et al* 1991, Fishkin and Gratton 1993, Fantini *et al* 1994a). Consequently, the usefulness of NIRS as a tool for *in vivo* measurement and monitoring has increased. One of the promising applications of NIRS is the monitoring of cerebral haemoglobin oxygen saturation and cerebral haemoglobin content in infants. Several studies have already established the usefulness of NIRS for the non-invasive measurement of saturation changes in infants (Sevick *et al* 1991, Cope and Delpy 1988, Edwards *et al* 1988). In addition, because of its large cerebral cortex, the piglet has been used as an animal model for the human infants in studies using all three basic categories of NIRS tissue spectrometers: continuous wave (CW) (Brun *et al* 1997, Stankovic *et al* 1998, Matcher *et al* 1995, Fantini *et al* 1999), frequency domain (FD) (Fantini *et al* 1999, Stankovic *et al* 1999, Du *et al* 1998, Ma *et al* 1999) and time domain (TD) (Yamashita *et al* 1996).

CW instruments measure only intensity. FD instruments use radiofrequency intensity-modulated light, and measure intensity, phaseshift and demodulation. TD instruments use pulsed light sources, and measure intensity, transient time and pulse shape. Most CW instruments assume that tissues have constant light scattering properties, and apply a fixed ‘differential path length factor’ (DPF) to account for tissue scattering. CW instruments are therefore unable to make quantitative absorption or haemoglobin measurements without *a priori* knowledge of DPF or scattering. FD and TD instruments make use of the additional information (phase or time) to measure scattering concurrently with absorption. However, single-distance instruments may be difficult to calibrate for *in vivo* concentration measurements.

Recently a frequency-domain multiple distance (FDMD) method was developed at the Laboratory for Fluorescence Dynamics (University of Illinois at Urbana-Champaign) for quantitative spectroscopy in highly scattering media (Fishkin and Gratton 1993, Fantini *et al* 1994a, b, Wallace *et al* 1999, Franceschini *et al* 1997). FDMD utilizes spatially resolved frequency-domain data to make absolute absorption and scattering measurements. It does not require *a priori* knowledge of the scattering properties of the sample, or the initial absorption values. Thus, the FDMD method is capable of quantitatively determining local tissue haemoglobin concentration and tissue haemoglobin oxygen saturation (StO<sub>2</sub>).

Since it is impractical to account for the true complexity of tissues, the theoretical model used for the FDMD method is based on an isotropic and macroscopically homogeneous sample. In addition, the accuracy of quantitative haemoglobin concentration measurements is hindered by a lack of knowledge concerning the absorption background (non-haemoglobin) in tissues. In brain tissue, haemoglobin, water and cytochrome-c oxidase are known chromophores in the near-infrared region (Matcher *et al* 1995), but the concentrations vary between individuals and the *in vivo* absorption spectra of cytochrome is difficult to measure precisely. It is also likely that there are other important chromophores, such as fats, that may make a significant contribution to the non-haemoglobin absorption. Quantitative absorption data for brain tissue,

in the wavelength range 700–850 nm, is relatively scarce. For these reasons, any NIRS method (especially a quantitative one) must be verified in real tissues via animal studies.

The experimental validation of quantitative  $StO_2$  measurements is confounded by the unknown relationship between  $StO_2$  measurements and the conventional values to which  $StO_2$  is readily compared; arterial saturation ( $SaO_2$ ) and venous saturation ( $SvO_2$ ). While  $StO_2$  is expected to lie between  $SvO_2$  and  $SaO_2$  (at least when  $SvO_2$  is measured locally), the relative contributions of  $SvO_2$  and  $SaO_2$  to  $StO_2$  are unknown, and they may change dynamically. In general the physiological meaning of  $StO_2$  is little understood (see for example Swain and Pittman (1989)).

We have performed a number of hypoxic stress tests in newborn piglets while monitoring brain haemodynamics with an FDMD-based tissue oximeter (ISS Oximeter, model 96208). The FDMD tissue-oximeter was used to measure tissue haemoglobin concentration and saturation in five piglets while inspired oxygen per cent ( $FiO_2$ ) was adjusted over a range of values to produce hypoxia (lower than normal saturation), normoxia (normal saturation) and hyperoxia (higher than normal blood oxygen saturation).  $SaO_2$  and  $SvO_2$  (from both the femoral vein and superior sagittal-sinus vein) were measured after each  $FiO_2$  change using conventional blood gas analysis. These studies were carried out to provide a set of data to compare NIR (FDMD) measured  $StO_2$  and haemoglobin concentration values with blood gas measurements ( $SvO_2$  and  $SaO_2$ ) over a range of tissue saturation.

Using the quantitative absorption values measured at two wavelengths, we have applied two different methods to determine quantitative haemoglobin concentration and  $StO_2$  values. In the first method we assume that background absorption is due only to 80% (by volume) water. Using this method, a direct comparison of  $StO_2$  with  $SvO_2$  and  $SaO_2$  can be made. In the second method, we assume that  $StO_2$  is equal to a fixed weighted average of  $SvO_2$  and  $SaO_2$  at normoxia and mild hypoxia. We then calculate the value of the background absorption that is required to satisfy this assumption of a fixed relationship. This is the empirical method described by Ma *et al* (1999).

Measured  $StO_2$  values were found to be linearly correlated with the average of the  $SvO_2$  and  $SaO_2$ . However, the water-only background assumption resulted in  $StO_2$  values that corresponded to a higher range of  $SvO_2$  to  $SaO_2$  ratios than seems reasonable.  $StO_2$  values shifted from close to the  $SaO_2$  values at low  $FiO_2$  levels, to near the  $SvO_2$  values at high  $FiO_2$  levels. In several instances,  $StO_2$  did not lie between  $SvO_2$  and  $SaO_2$ , with  $StO_2$  values greater than  $SaO_2$  at very low  $FiO_2$ , and less than  $SvO_2$  at high  $FiO_2$ .

The application of the background measurement method of Ma *et al* (1999) resulted in estimated background values much higher than those expected for water and cytochrome-c oxidase. While we cannot conclude that this is the ‘true’ absorption background for piglet brain tissue, we can say that ‘effective’ background appears to be larger than expected for FDMD measurements on piglet heads.

## 2. Theory and instrumentation

### 2.1. The frequency-domain multiple-distance method

The theoretical principles of the FDMD method have been previously described. A brief overview is presented here for the sake of clarity, and to define certain terminology.

As light travels outward from a ‘point source’ in a highly scattering medium, the radiant energy density,  $U$ , decreases more than exponentially with increasing distance from the source. In frequency-domain instruments, the intensity of the light source(s) is sinusoidally modulated. A ‘photon density wave’ can be said to propagate through the medium outward from the source.

The variation in time of radiant energy density at any point in the medium can be described by the equation

$$U(t) = U_{AC} \sin(2\pi ft + \Phi_U) + U_{DC} \quad (1)$$

where  $U_{AC}$  is the amplitude of the modulation in the energy density,  $f$  is the frequency of the modulation,  $\Phi_U$  is the phase and  $U_{DC}$  is the average radiant energy density. Both  $U_{AC}$  and  $U_{DC}$  decrease as a function of the distance between the point of observation and the source. While the photon density wave travels with a constant speed, the speed of the photon density wave is slower than the speed of light in the medium ( $v$ ). The phase at a fixed time increases with distance according to the propagation speed of the photon density wave. The rate of change in  $U_{AC}$ ,  $U_{DC}$  and  $\Phi_U$  with distance are functions of the optical properties of the medium including  $\mu_a$  and  $\mu'_s$ . The absorption coefficient ( $\mu_a$ ) is the inverse mean distance a photon travels before it is absorbed. The absorption coefficient has units of reciprocal distance, and is typically  $0.05\text{--}0.3\text{ cm}^{-1}$  for tissues in the wavelength region between 700 nm and 900 nm. The reduced scattering coefficient ( $\mu'_s$ ) is a measure of scattering per unit distance, and is typically  $4\text{--}15\text{ cm}^{-1}$  for tissues. The reduced scattering coefficient is equal to  $\mu_s(1 - g)$ , where  $\mu_s$  (the scattering coefficient) is the inverse mean distance a photon travels between consecutive scattering events, and  $g$  is the average of the cosine of the scattering angle. The reduced scattering coefficient refers to effectively isotropic scattering events and it is given by the inverse of the mean distance over which a photon loses memory of its original direction of propagation. In tissues, the  $\mu'_s$  is typically one order of magnitude greater than  $\mu_s$ .

Fishkin and Gratton (1993) have derived simple relationships for FDMD measurements in an infinite turbid medium. These equations are based on the ‘diffusion approximation’ to the Boltzmann transport equation (which cannot be solved ‘analytically’), and were derived using approximations based on the condition that reduced scattering coefficient is much larger than absorption coefficient ( $\mu'_s \gg \mu_a$ ), that the source–detector separation distance ( $r$ ) is much larger than the average distance between scattering events ( $r \gg 1/\mu_s$ ), and that modulation frequency is much smaller than the scattering rate ( $2\pi f \ll v\mu'_s$ ). Fantini *et al* (1994a) have extended the derivation to find relationships that apply at the ‘surface’ of a semi-infinite medium (an infinite medium bounded by a flat plane). However, Fantini *et al*’s original equations required an iterative solution. Liu *et al* (1995a) suggested an approximation based on the condition  $r \gg 1/(\mu'_s + \mu_a)$ . We have taken a similar approach and made the approximation that  $r(3\mu_a\mu'_s)^{1/2} \gg 1$ . The value of  $r(3\mu_a\mu'_s)^{1/2}$  is typically greater than 2.5 for distances greater than 1.5 cm in brain tissue. For example for  $\mu_a = 0.1\text{ cm}^{-1}$   $\mu'_s = 10\text{ cm}^{-1}$  and  $d = 1.5\text{ cm}$  this quantity is 3.2. When this approximation is applied to Fantini *et al*’s relationships, the resulting equations are greatly simplified. While the more exact equations given by Fantini are slightly more accurate, this more approximate solution does not require the use of iterative calculations, and it is therefore more easily applied to rapid ‘real-time’ computation.

The following equations are based on Fantini *et al*’s equations with  $r(3\mu_a\mu'_s)^{1/2} \gg 1$ . They describe how the time average ( $R_{dc}$ ), modulation amplitude ( $R_{ac}$ ) and phaseshift ( $R_\Phi$ ) of the detected signal changes with source–detector distance ( $r$ ) for a sinusoidally modulated ‘point’ light source:

$$\ln(R_{dc}r^2) = rS_{dc}(\mu_a, \mu'_s) + I'_{dc}(D, K_{dc}) \quad (2)$$

with

$$S_{dc} = -(\mu_a/D)^{1/2} \quad (3)$$

$$R_\Phi = rS_\Phi(\mu_a, \mu'_s, \omega, v) + I'_\Phi(K_\Phi) \quad (4)$$

with

$$S_{\Phi} = \left(\frac{\mu_a}{2D}\right)^{1/2} \left\{ \left[ 1 + \left(\frac{\omega}{v\mu_a}\right)^2 \right]^{1/2} - 1 \right\} \quad (5)$$

and

$$\ln(R_{ac}r^2) = rS_{ac}(\mu_a, \mu'_s, \omega, v) + I'_{ac}(D, K_{dc}) \quad (6)$$

with

$$S_{ac} = -(\mu_a/2D)^{1/2} \left\{ \left[ 1 + \left(\frac{\omega}{v\mu_a}\right)^2 \right]^{1/2} + 1 \right\}^{1/2}. \quad (7)$$

In these equations,  $v$  is the speed of light in the medium and  $\omega$  is the angular frequency of the modulation.  $D$  is the diffusion coefficient, where  $D = 1/(3\mu_a + 3\mu'_s)$  (which is approximately  $1/(3\mu'_s)$  since  $\mu'_s \gg \mu_a$ ).  $K_{dc}$  and  $K_{ac}$  are constants that depend on source intensity, modulation depth, detector sensitivity factors and other instrumental factors.  $K_{\Phi}$  is the relative phase of the source plus any phaseshifts external to the sample.

To facilitate the multidistance method, equations (2), (4) and (6) are written so that the quantity on the left of the equality has a linear dependence on  $r$ .  $S_{dc}$  denotes the slope of the line obtained when  $\ln(R_{dc}r^2)$  is plotted against  $r$ ,  $S_{ac}$  denotes the slope of the line defined by  $\ln(R_{ac}r^2)$  versus  $r$ , and  $S_{\Phi}$  is the slope of the line defined by  $\Phi$  versus  $r$ .  $I'_{dc}$ ,  $I'_{ac}$  and  $I'_{\Phi}$  define the intercepts of the lines and are functions of  $D$  and instrumental factors (Fantini *et al* 1994a).

Note that the slopes  $S_{ac}$ ,  $S_{dc}$  and  $S_{\Phi}$ , are independent of the instrumental parameters  $K_{dc}$ ,  $K_{ac}$  and  $K_{\Phi}$ . In practice  $R_{ac}$ ,  $R_{dc}$  and  $R_{\Phi}$  are measured at several source–detector separations ( $r$ ) and  $S_{ac}$ ,  $S_{dc}$  and  $S_{\Phi}$  are found by linear regression. Next,  $\mu_a$  and  $\mu'_s$  are recovered by solving the system of simultaneous linear equations defined by the three ‘slope functions’ given in equations (3), (5) and (7). Since there are two unknowns and three equations, any two slopes can be used. However, the small difference between  $S_{ac}$  and  $S_{dc}$  observed in tissues using 110 MHz modulation prevents the practical use of this pair. The  $S_{ac}$  and  $S_{\Phi}$  pair is preferred, since  $S_{ac}$  is less affected by room light. Although these approximate equations have several limitations, they have been experimentally verified in media with ‘tissue-like’ optical properties (Fantini *et al* 1994a, b, 1995).

If  $\mu'_s$  is constant, equations (3) and (7) can each be solved directly for  $\mu_a$ , requiring only that  $S_{ac}$  or  $S_{dc}$  be continuously measured. That is, the initial  $\mu'_s$  values can be calculated based on the initial intensity ( $R_{ac}$  or  $R_{dc}$ ) and phase values, and thereafter only intensity need be measured. This approach can be useful, because phase noise is often the dominant noise source in frequency-domain spectroscopic measurements; however, it is not accurate when scattering changes significantly. In this study, a compromise solution was used (Wallace *et al* 1999). Equations (5) and (7) were used to solve for  $\mu'_s$ , but an additional moving average was applied to the resulting values, before equation (7) was used to find  $\mu_a$ . It is assumed that large changes in  $\mu'_s$  occur slowly (several seconds), and this is usually the case for brain measurements. Even if there are fast changes in  $\mu'_s$ , only transient anomalies in  $\mu_a$  result. In addition, the absence of large changes in scattering can be confirmed by comparing fast  $\mu'_s$  measurements with  $\mu'_s$  with the additional averaging.

Once  $\mu_a$  has been determined at two or more near-infrared wavelengths, the concentration of oxyhaemoglobin [oxy-Hb] and deoxyhaemoglobin [deoxy-Hb] can be determined based on the Beer–Lambert law. These values are in turn used to find the total haemoglobin concentration [total-Hb] and the per cent mole fraction of oxyhaemoglobin,  $StO_2 = [\text{oxy-Hb}]/[\text{total-Hb}] \times 100\%$ .  $StO_2$ , as measured by NIR spectroscopy, is due mostly to the blood found in capillaries, with some contribution from arterioles and venules (Liu *et al* 1995b).  $StO_2$  can be modelled as a weighted average of arterial saturation and the local venous saturation.

However, since saturation in a large region of small vessels cannot be directly measured by other means, the exact relationship between  $\text{StO}_2$  and the saturation in larger vessels is not known.

The use of the Beer–Lambert law to calculate both [oxy-Hb] and [deoxy-Hb] based on the absorption at only two wavelengths requires that the measured absorption coefficients be corrected for by subtraction of the ‘background absorption’, where the ‘background absorption’ is the sum contribution to the absorption coefficients of all non-haemoglobin tissue components. In this study, we first made the simplifying presumption that haemoglobin and water were the only significant absorbers. However, our results, and those of previous measurements, suggest that the actual background absorption may be much larger in the piglet head. Therefore, we have also used the empirical method essentially similar to that described by Ma *et al* (1999) to estimate the background directly.

Using this empirical method, the background absorption is found by creating a perturbation in saturation (via hypoxia), and then calculating the background necessary to adjust the recalculated  $\text{StO}_2$  values to an assumed weighted average of  $\text{SvO}_2$  and  $\text{SaO}_2$ . For simplicity, a fixed mixture of 1:1 (50%  $\text{SvO}_2$  and 50%  $\text{SaO}_2$ ) was chosen. That is, the average of  $\text{SvO}_2$  and  $\text{SaO}_2$  was used. Ma and co-workers used normoxia and a moderate hypoxia as the two saturation states. While, mathematically, more precision could be achieved by using extreme hypoxia, a larger change in apparent mixture of  $\text{SvO}_2$  and  $\text{SaO}_2$  would be expected due to vascular dilation. In Ma *et al*'s study, a change in  $\text{SaO}_2$  of about 40% and  $\text{SvO}_2$  of 30% was induced by a  $\text{FiO}_2$  change from 30% to 15%. In the present study, a larger range of  $\text{FiO}_2$  (27–10%) was required to achieve a comparable change in  $\text{SvO}_2$  and  $\text{SaO}_2$ .

The basis of this empirical background method is simple. From the Beer–Lambert law, the familiar solution for two principal absorbers can be written to include fixed background absorption:

$$[\text{oxy-Hb}] = \frac{\varepsilon_{\text{deoxy-Hb}}(\lambda_2)\{\mu_a(\lambda_1) - B(\lambda_1)\} - \varepsilon_{\text{deoxy-Hb}}(\lambda_1)\{\mu_a(\lambda_2) - B(\lambda_2)\}}{\ln(10)\{\varepsilon_{\text{deoxy-Hb}}(\lambda_2)\varepsilon_{\text{oxy-Hb}}(\lambda_1) - \varepsilon_{\text{deoxy-Hb}}(\lambda_1)\varepsilon_{\text{oxy-Hb}}(\lambda_2)\}} \quad (8)$$

and

$$[\text{deoxy-Hb}] = \frac{\varepsilon_{\text{oxy-Hb}}(\lambda_1)\{\mu_a(\lambda_2) - B(\lambda_2)\} - \varepsilon_{\text{oxy-Hb}}(\lambda_2)\{\mu_a(\lambda_1) - B(\lambda_1)\}}{\ln(10)\{\varepsilon_{\text{deoxy-Hb}}(\lambda_2)\varepsilon_{\text{oxy-Hb}}(\lambda_1) - \varepsilon_{\text{deoxy-Hb}}(\lambda_1)\varepsilon_{\text{oxy-Hb}}(\lambda_2)\}} \quad (9)$$

where  $\varepsilon_x$  are the extinction coefficients,  $B$  is the background absorption and  $\lambda_1$  or  $\lambda_2$  indicates the wavelength. The  $\ln(10)$  is required because the extinction coefficients ( $\text{cm}^{-1} \text{M}^{-1}$ ) are based on the base 10 exponential expression of the Beer–Lambert law, whereas the absorption coefficient used in diffusion theory is related to the base  $e$  exponential form (i.e.  $10^{(-\varepsilon cd)} = e^{(-\mu_a d)}$  and  $\mu_a = \ln(10)\varepsilon c$ , where  $c$  is concentration and  $d$  is path length). By combining these equations we can find the relationship between the ratio of [oxy-Hb] to [deoxy-Hb] in terms of known extinction coefficients, measured absorption coefficients and the unknown background absorption coefficients:

$$\frac{[\text{oxy-Hb}]}{[\text{deoxy-Hb}]} = \frac{\varepsilon_{\text{deoxy-Hb}}(\lambda_2)\{\mu_a(\lambda_1) - B(\lambda_1)\} - \varepsilon_{\text{deoxy-Hb}}(\lambda_1)\{\mu_a(\lambda_2) - B(\lambda_2)\}}{\varepsilon_{\text{oxy-Hb}}(\lambda_1)\{\mu_a(\lambda_2) - B(\lambda_2)\} - \varepsilon_{\text{oxy-Hb}}(\lambda_2)\{\mu_a(\lambda_1) - B(\lambda_1)\}}. \quad (10)$$

Note that

$$\frac{[\text{oxy-Hb}]}{[\text{deoxy-Hb}]} = \frac{\text{StO}_2}{1 - \text{StO}_2}.$$

By considering two points (normoxia and mild hypoxia) with unequal saturation values, two simultaneous equations based on equation (10) can be written. The two values of  $\text{StO}_2$  (and thereby [oxy-Hb]/[deoxy-Hb]) can be estimated using the average of the measured  $\text{SvO}_2$

and  $SaO_2$  values, and the simultaneous equations can be solved for the background absorption coefficients,  $B(\lambda_1)$  and  $B(\lambda_2)$ .

It should be emphasized that this empirical background method is based on three assumptions:

- (a) The  $StO_2$  is equivalent to a mixture of 50%  $SvO_2$  and 50%  $SaO_2$  during both normoxia and mild hypoxia.
- (b) the background absorption is constant.
- (c) The method used to measure tissue absorption (in this case FDMD) is accurate.

While these assumptions limit the accuracy of the method, the resulting values are still useful for judging the possible significance of the background absorption. Also, small changes in the assumed mixture of  $SvO_2$  and  $SaO_2$  have only a small effect on the resulting background values. However, without independent verification, the resulting background values are best seen as empirically determined absorption correction terms, since this method cannot distinguish between real background absorption and systematic errors that lead to constant positive offsets in the measured absorption coefficients.

## 2.2. The tissue oximeter

A dual channel tissue oximeter (model 96208, ISS, Inc., Champaign, IL) was used for this study. This instrument has been described previously in the literature (Wallace *et al* 1999, Franceschini *et al* 1997).

The tissue oximeter contained laser diode sources and photomultiplier tube (PMT) detectors. All sources and detectors were fibre-optically coupled to the sample probe. In this study, eight sources (four that emitted at 758 nm and four that emitted at 830 nm), and one detector were used. The laser diodes were intensity modulated at 110 MHz and were multiplexed such that only one source was 'on' at a time. All eight sources were switched on and off in a continuous cycle. While each source was on,  $R_{ac}$ ,  $R_{dc}$  and  $R_{\Phi}$  were measured. One cycle of all eight sources required only 160 ms. The software allowed for real-time acquisition, calculation, display and storage of all the 'raw' ( $R_{ac}$ ,  $R_{dc}$  and  $R_{\Phi}$  values) data plus  $S_{ac}$ ,  $S_{dc}$ ,  $S_{\Phi}$ ,  $\mu_a$ ,  $\mu'_s$ , [oxy-Hb], [deoxy-Hb], [total-Hb] and  $StO_2$ .

## 2.3. The optical probe

The optical probe used for this study was designed specially to overcome the problems caused by the rough surface and the thick stiff hair on a piglet's head, and it was similar to a probe used for a previous study (Fantini *et al* 1999, Stankovic *et al* 1999). The probe was based on a rectangular, 8 mm thick aluminium plate attached to an aluminium rod for mounting. The probe contained two parallel rows of source (light emitting) fibre-optics (400  $\mu\text{m}$  core diameter), and one fibre-optic (light collecting) detector bundle (3 mm diameter) placed at the end of the rows of emitters fibres. Four emitters fibres (one row) were connected to 758 nm lasers and the other four were connected to 830 nm lasers (see figure 1).

The source fibres were not fixed in place. The emitting tips were 'clad' with stainless steel tubing and slid into holes in an aluminium block. The source fibres could be pushed downwards with a slight force, ensuring consistent contact between the tips of the fibre-optics and the skin. The input tip of the detector bundle was fixed in place about 2–3 mm below the plane of the probe, and the tip was bevelled at  $15^\circ$  to help match the shape of the piglets' heads. To block surface-reflected light (emitted by a source fibre), a piece of black foam was glued to the bottom of the probe between the collector bundle and emitter fibres. The probe was held in place by a system of posts and clamps.

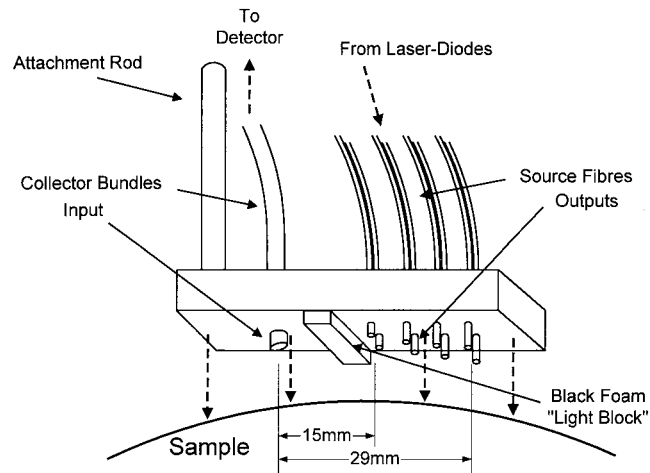


Figure 1. Illustration of the frequency-domain multiple-distance (FDMD) optical probe used.

### 3. Experiment

#### 3.1. Oximeter calibration

Because the oximeter's multiple sources do not emit with equal intensity or phase, an instrumental calibration must be performed to correct these inequalities. The calibration procedure is simple and requires less than 3 min. The optical probe was placed on a previously measured calibration phantom. The ratios of the ac and dc intensities and the relative phase ( $\Phi$ ) difference between signals arising from each location were compared with the ratios and differences predicted by equations (3), (5) and (7). The calibration values needed to correct the intensities and phases of each of the sources were calculated, and these corrective values were stored by the software for later application during subsequent measurements.

To facilitate consistent contact between the emitting tips of the fibre-optic and the surface of the phantom, the phantom was made of a pliable RTV silicon resin. To obtain tissue-like optical properties,  $\text{TiO}_2$  (1  $\mu\text{m}$  average particle size) and carbon black powders were added to the resin before it was moulded into a roughly  $15 \times 10 \times 10 \text{ cm}^3$  block. To more closely match the shape of the piglets' heads, one side of the calibration phantom was cylindrically curved with a radius of curvature of 15 cm.

The calibration phantom used for this study had optical properties of  $\mu_a = 0.113 \text{ cm}^{-1}$  at 758 nm,  $\mu_a = 0.105 \text{ cm}^{-1}$  at 830 nm,  $\mu'_s = 10.5 \text{ cm}^{-1}$  at 758 nm and  $\mu'_s \text{ cm}^{-1} = 9.68 \text{ cm}^{-1}$  at 830 nm. These properties had been previously determined by measurements using a single movable source and a single detector.

While this calibration might be seen as a calibration against known optical properties, it is more correctly seen as an instrumental calibration independent of the particular values of the optical properties of the calibration phantom. In fact, the same theory is used to calculate both the optical properties of the calibration phantom and the calibration correction values. Therefore, the calibration procedure has, in reality, the purpose of matching the intensity and phase dependence on distance measured with multiple sources, with those measured using a single source. When a true standard material for calibration of quantitative absorption and scattering measurements becomes available, calibration against known optical properties will be possible.



### 3.2. Animal protocol

We measured five piglets. Each piglet was anaesthetized (5% halothane + nitrous oxide, with  $25 \mu\text{g kg}^{-1}$  fentanyl for pain) and intubated. An incision was made in the scalp about 2 mm to the right of the sagittal structure (midline) of the skull, and a small hole was made near the midline of the skull. The superior sagittal-sinus (vein) was catheterized for subsequent blood gas measurements. Also, a femoral cut-down was performed to insert catheters into the inferior femoral vein and artery for periodic arterial and femoral venous blood gas monitoring. The blood pressure, heart rate and arterial oxygenation of each piglet were monitored continuously. The latter was monitored using a Nellcor model N-200 pulse oximeter, with the probe attached to the piglet's tail. The tissue oximeter's auxiliary-device input system was used to monitor the outputs of the pulse oximeter, so that arterial saturation and heart rate could be recorded along with the data from tissue oximeter. Finally, a strain gauge belt (Sleepmate/Newlife Technologies, Resp-EZ) was used to monitor breathing, and its output was also attached to the auxiliary-device input system of the tissue-oximeter.

The scalp incision was closed with cyanoacrylate adhesive and tape. The non-invasive probe of the tissue oximeter was placed on the top of the piglet's head (to the left of the incision), about 1.5–2.0 cm from the sagittal structure (midline) of the skull. It was held in place with a system of posts and clamps. The piglet's head was held in position only by the slight downward force of the oximeter probe. No special precautions were needed to prevent motion artefacts. The optical source fibres were attached to the clamps such that the output tip of each fibre output tip was held against the piglet's head with a slight downward pressure.

Once the piglet was stabilized, a 'base line' was measured for a few minutes, with the initial ventilator gas mixture adjusted to provide approximately 27%  $\text{FiO}_2$  and a breathing rate of 30–35  $\text{min}^{-1}$ . Blood was drawn from the superior sagittal-sinus, femoral vein and femoral artery for initial blood gas measurements (Ciba-Corning model 280 gas analyser). Thus, four haemoglobin oxygen saturation indices were measured: SS-SvO<sub>2</sub> (sagittal-sinus venous saturation), fem-SvO<sub>2</sub> (femoral venous saturation), SaO<sub>2</sub> (arterial saturation) and NIRS StO<sub>2</sub> (tissue saturation). The pulse oximeter supplied an additional measure of arterial saturation (PO-SaO<sub>2</sub>). However, the data from the pulse oximeter were not always available, since the device failed to provide consistently stable output during the study.

After the initial measurements,  $\text{FiO}_2$  was changed in steps. Each value of  $\text{FiO}_2$  was maintained for at least 3 min. New blood gas readings were obtained 3–5 min after each change in  $\text{FiO}_2$ . Since a large total volume of blood was drawn, a saline solution was used to maintain blood volume. The following pattern of  $\text{FiO}_2$  levels was used for piglets 1–3: cycle 1,  $\text{FiO}_2 \approx 27\% - 15\% - 10\% - 27\%$ ; cycle 2,  $\text{FiO}_2 \approx 27\% - 15\% - 10\% - 27\%$ ; cycle 3,  $\text{FiO}_2 \approx 27\% - 15\% - 10\% - 5\% - 90\% - 27\%$ . Cycle 2 was identical to cycle 1, but cycle 3 included two more extreme  $\text{FiO}_2$  levels, including severe hypoxxygenation (5%  $\text{FiO}_2$ ), and hyperoxygenation (90%  $\text{FiO}_2$ ). The same pattern was used for piglets 4 and 5, except that cycle 3 was omitted. Tissue oximeter measurements were made continuously during each cycle.

### 3.3. Data analysis

The data files were 'marked' at each moment that blood was drawn for blood gas measurements. These file markers were later used to correlate blood gas measurements with the time index in the continuous StO<sub>2</sub> record. File markers were also placed whenever a change in  $\text{FiO}_2$  was initiated, and on completion of the change.

Absorption and concentration values were measured at a rate of 6.25 Hz (160 ms per measurement), and scattering was measured at 0.156 Hz (6.4 s per measurement). The index

of refraction in the tissue was taken as 1.4, and the data for haemoglobin extinction-coefficient were taken from Wray *et al* (1988). During the real-time analysis, the sample was assumed to consist of 80% water by volume, and it was assumed that the only background absorption was that due to water.

Empirical background absorption values were calculated (after the experiment) using a technique similar to that described by Ma *et al* (1999), as outlined in section 2.1 above. These values were then used to recalculate [oxy-Hb], [deoxy-Hb], [total-Hb] and StO<sub>2</sub> for each piglet. The average (for piglets 2–5) empirical background absorption values were also used to explore the effect of differences in measured background for each piglet. In each case, the first (27%) and third (10%) FiO<sub>2</sub> steps in the cycle were used as the two saturation points introduced in section 2.1 above.

## 4. Results and discussion

### 4.1. Results using water-only background absorption

Good linearity was found in most cases for the lines used to define the slopes  $S_{ac}$ ,  $S_{dc}$  and  $S_{\phi}$ . The square of the linear regression correlation coefficient ( $R^2$ ) was better than 0.99 in most cases. One exception was for piglet 2, where  $R^2$  was 0.96 for  $S_{ac}$  at 758 nm. For piglet 1, bad linearity ( $R^2 < 0.98$ ) was found for several of the lines. Furthermore, the linearity worsened during the course of the experiment. This indicates that the theoretical model was not appropriate and that the measured slopes ( $S_{ac}$ ,  $S_{dc}$  and  $S_{\phi}$ ) were not reliable for piglet 1. This lack of a fit to theory may be attributed to an uneven distribution of blood beneath the optical probe. At the conclusion of the procedure, it was noted that the surgery performed on piglet 1's head caused copious bleeding, and blood was found between the scalp and the probe. In addition, the results for piglet 1 were dissimilar from those seen for piglets 2–5. Therefore, no data from piglet 1 have been included in any average value reported in this study.

Figure 2 shows the traces obtained during the three FiO<sub>2</sub> cycles run with piglet 3 (A, B, C, D, cycle 1; E, F, G, H, cycle 2; and I, J, K, L, cycle 3). For all these plots, it was assumed that the only absorption background was due to 80% water by volume. Parts A, E and I show the four saturation indices, SaO<sub>2</sub> measured with the gas analyser and with the pulse oximeter (po-SaO<sub>2</sub>), and SvO<sub>2</sub> measured in blood from both the femoral vein (fem-SvO<sub>2</sub>) and the sagittal-sinus (SS-SvO<sub>2</sub>), and StO<sub>2</sub>. The average baseline StO<sub>2</sub> for piglets 2–5 was 58.5% with a standard deviation of 2%. As expected, there is a good qualitative correlation between StO<sub>2</sub> and both SvO<sub>2</sub> and SaO<sub>2</sub>. A striking feature is the 'overshoot' in StO<sub>2</sub> coinciding with changes from low FiO<sub>2</sub> to high FiO<sub>2</sub>. Notice also that SS-SvO<sub>2</sub> is significantly lower (by more than 10% in many cases) than fem-SvO<sub>2</sub> at all times except for hyperoxygenation (90% FiO<sub>2</sub>) and extreme hypoxxygenation (5% FiO<sub>2</sub>), when the difference between SaO<sub>2</sub> and SvO<sub>2</sub> is small. Since the superior sagittal-sinus blood is a closer approximation to local venous blood, we have concentrated on an analysis of the relationship between StO<sub>2</sub>, SS-SvO<sub>2</sub> and SaO<sub>2</sub>.

Saturation values show some trend with cycle number, especially at 15% FiO<sub>2</sub> (the mildest hypoxia). SS-SvO<sub>2</sub> drops from a 70% value during the first period of 15% FiO<sub>2</sub> (cycle 1), to 53% during the second period of 15% FiO<sub>2</sub>, to 40% during the third period of 15% FiO<sub>2</sub>. SaO<sub>2</sub> and StO<sub>2</sub> also decrease. The reason for these differences is unknown. It may be a result of anaesthesia, injury caused by the changes in FiO<sub>2</sub> or a slight ischaemia (caused by the removal of blood for the multiple blood gas measurements). However, the cause of these changes is beyond the scope of this study.

Figure 2 parts B, F, J show the haemoglobin concentration measurements. The average initial total haemoglobin concentration ([total-Hb]) was 0.063 mM (in piglets 2–5) with a standard deviation of 0.014 mM. Note that small changes in StO<sub>2</sub> were not generally accom-

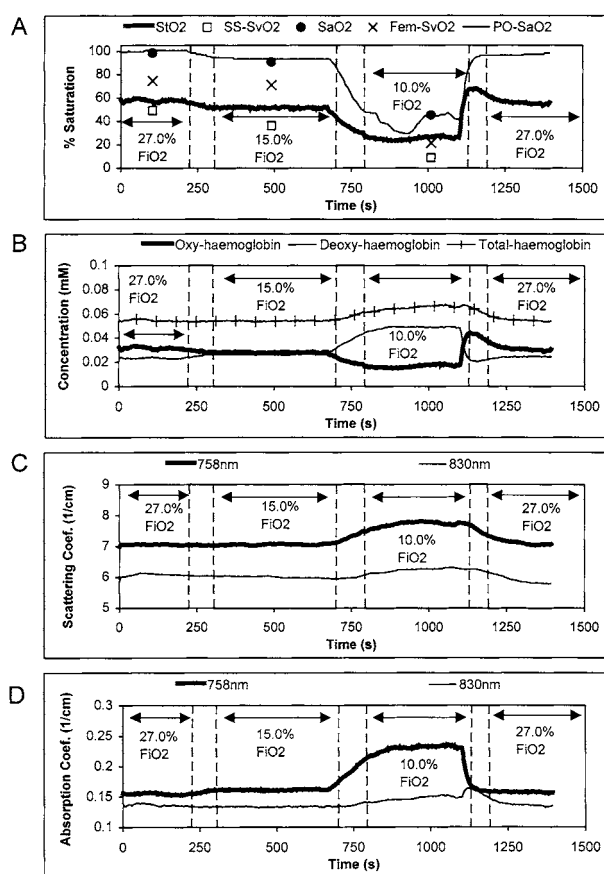


**Figure 2.** Time traces of measurements on piglet 3. Blood gas values are represented by points, and the broken vertical lines indicate the beginning and end of each FiO<sub>2</sub> level. Parts A–D were recorded during FiO<sub>2</sub> cycle 1, E–H during cycle 2 and I–L during cycle 3. Due to the large number of data points, the average of every eight values is shown.

panied by significant changes in [total-Hb]. However, larger decreases in StO<sub>2</sub> coincided with significantly increased [total-Hb], consistent with the expected vascular dilation and increased heart rate. Lower blood pressure and increased heart rate were observed at these times.

Figure 2 parts C, G and K indicate that scattering changed little during the experiments, except for an increase that coincided with the increase in [total-Hb] during hypoxigenation. It is interesting that the ‘overshoots’ in StO<sub>2</sub> measured when FiO<sub>2</sub> levels were adjusted from low to high levels are accompanied only with a gradual return of [total-Hb] and scattering to baseline levels. The average  $\mu'_s$  values for piglets 2–5 were 8.2 cm<sup>-1</sup> at 758 nm and 7.3 cm<sup>-1</sup> at 830 nm. The standard deviations in measured  $\mu'_s$  values were 1.7 cm<sup>-1</sup> and 2 cm<sup>-1</sup> at 758 nm and 830 nm respectively. The ratio of the  $\mu'_s$  values at 758 nm to 830 nm was 1.15:1 with a standard deviation of 0.1. An increase in scattering of 0.3–1 cm<sup>-1</sup> was typically observed under extreme hypoxia.

Figure 2 parts D, H and L show the measured absorption coefficients during the experiment on piglet 2, and figure 3 summarizes the saturation data for pigs 2–5 in one bar graph. The ‘error bars’ in this graph indicate one standard deviation for the entire set of measurements (all three FiO<sub>2</sub> cycles) for piglets 2–5. Note that there were only two samples at 90% and 5%

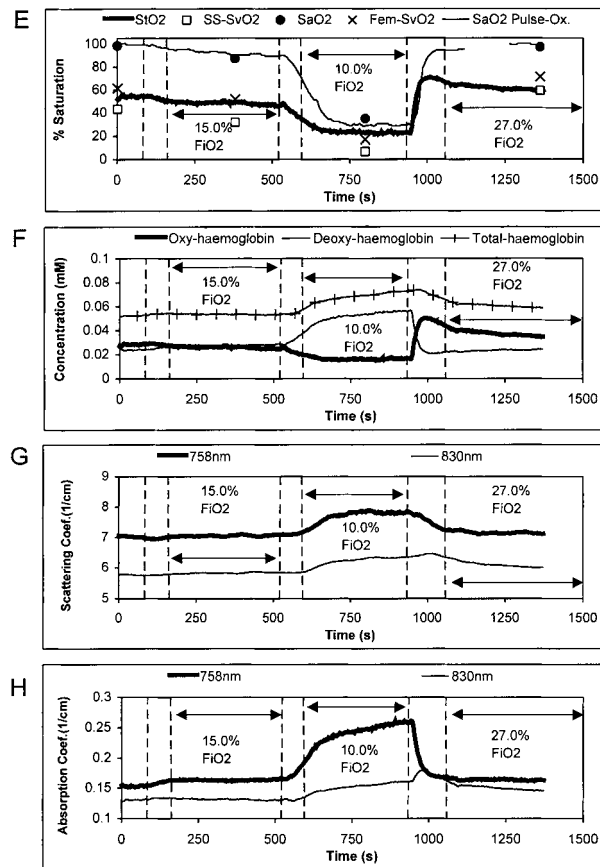


Figure 2. (Continued)

$F_{iO_2}$  (these 'error bars' represent the range of values) and that the last two bar types in figure 3 are discussed in section 4.3 below.

It might be surprising that the standard deviations of  $SaO_2$ ,  $SS-SvO_2$  and  $fem-SvO_2$  at 15%  $F_{iO_2}$  are larger than the standard deviation of the corresponding  $StO_2$  measurements. Clearly, the 'error-bars' do not indicate experimental error. Rather, there is much individual variation in response, particularly during mild hypoxia.

Figure 4 shows another view of the data. Here  $StO_2$  is correlated to the average of  $SS-SvO_2$  and  $SaO_2$ . The straight line was found by linear regression analysis. The three  $F_{iO_2}$  cycles are represented with diamonds, squares and triangles respectively. Only a slight pattern based on cycle number is evident in this figure. During cycle three, almost all points lie below the line. This may indicate that the relationship between  $StO_2$  and the blood gas measurements may change slightly during the experiment. However, this difference is small and may be due to experimental errors, instrument drift or a physiological change. The fact that there is a nearly linear correlation between  $StO_2$  and the average of  $SS-SvO_2$  and  $SaO_2$  is significant. In fact, there is a nearly linear correlation between  $StO_2$  and any reasonable (from 15% venous to 100% venous) weighted average of  $SS-SvO_2$  and  $SaO_2$ .

It is well known that neither venous nor arterial saturation changes linearly with respect to inspired oxygen or with respect to each other. For illustration and for comparison with

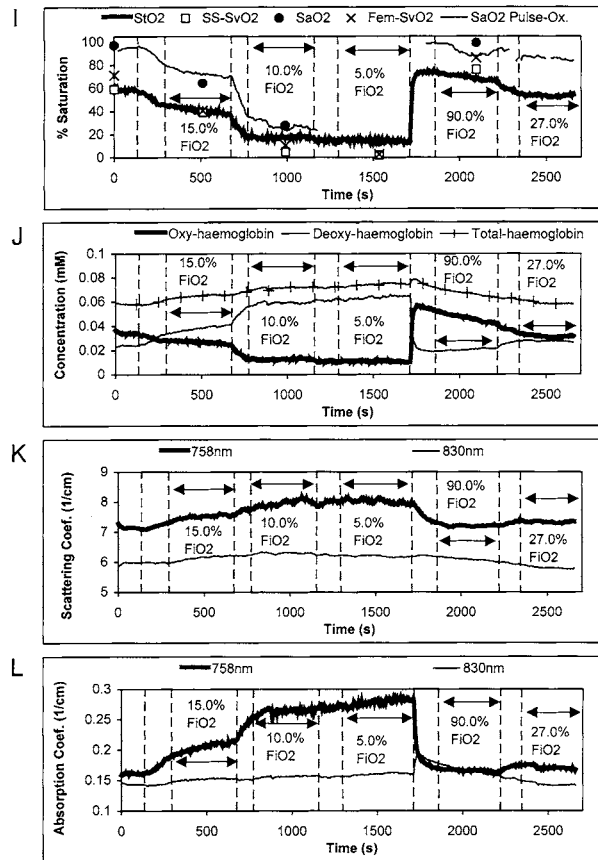


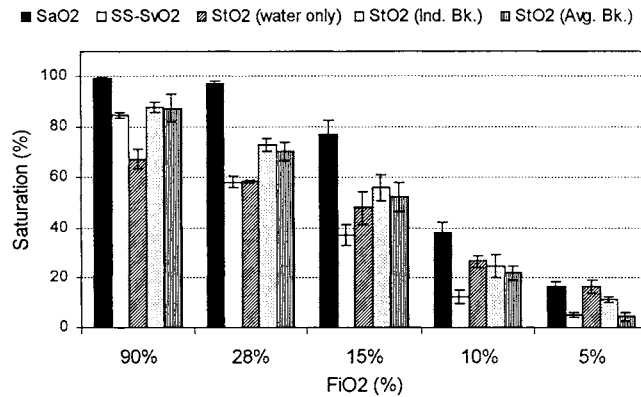
Figure 2. (Continued)

figure 4, figure 5 shows the correlations between SS-SvO<sub>2</sub> and SaO<sub>2</sub> against the average of SS-SvO<sub>2</sub> and SaO<sub>2</sub>. Of course, these blood gas values are strongly correlated to their own average, but clearly not linearly. The linearity of StO<sub>2</sub> with respect to the average of SS-SvO<sub>2</sub> and SaO<sub>2</sub> with a slope different from unity seems to indicate that the relationship between StO<sub>2</sub> to SaO<sub>2</sub> and SS-SvO<sub>2</sub> changes in a manner that coincidentally maintains a linear correlation.

Because of the linear relationship between measured StO<sub>2</sub> and the average of SS-SvO<sub>2</sub> and SaO<sub>2</sub>, the average of arterial and venous saturation can be estimated by the simple empirical expression  $(StO_2 - b)/m$ , where  $m$  is the slope of the ‘best-fit’ line in figure 4, and  $b$  is the intercept. In this study,  $m$  was found to be 0.646 and  $b$  was 9.806%. In addition, one may derive an empirical formula for the variable mixture of SS-SvO<sub>2</sub> and SaO<sub>2</sub> that would provide a perfect one-to-one correlation with StO<sub>2</sub>. If  $StO_2 = X \times (SS-SvO_2) + [1 - X] \times SaO_2$ , then given the above empirical expression

$$X = \text{fraction SS-SvO}_2 = \frac{StO_2 - SaO_2}{2(StO_2 - SaO_2)m - b} m. \quad (11)$$

This equation suggests that one may predict local venous saturation in healthy tissue based on SaO<sub>2</sub> and local StO<sub>2</sub> (which may both be measured non-invasively). However, equation (11) is only an empirical relationship that fits this limited series of hypoxic stress



**Figure 3.** Average saturation indices for piglets 2-5, all FiO<sub>2</sub> cycles included. Bars labelled StO<sub>2</sub> (water only) are based on the assumption the water is the only significant background absorber. StO<sub>2</sub> (ind. bk.) indicates values recalculated with individual determined background absorption, and StO<sub>2</sub> (avg. bk.) indicates values based on the average background absorption for the four piglets (2-5). The 'error-bars' in this graph indicate one standard deviation for the entire set of measurements (piglets 2-5, all three FiO<sub>2</sub> cycles). Note that there were only two values each at 90% and 5% FiO<sub>2</sub>. The 'error-bars' for 90% and 5% FiO<sub>2</sub> represent the range of measured values.

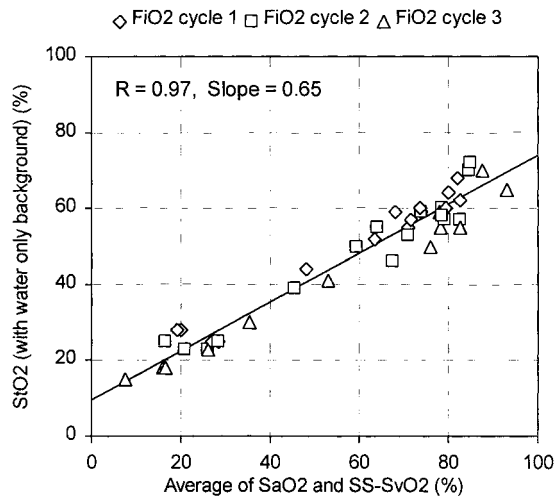


**Figure 4.** Correlation of StO<sub>2</sub> with the average of SaO<sub>2</sub> and SS-SvO<sub>2</sub>. The line indicates the result of linear regression.

experiments. Further validation is required before it can be applied to any other set of measurements.

#### 4.2. Anomalies in StO<sub>2</sub> (using water-only background assumption)

There are several anomalies in the StO<sub>2</sub> measured considering a water-only background. First the baseline values (58.5%) seem low, although similar baseline StO<sub>2</sub> values were observed in a previous piglet study using the same FDMD instrument (Fantini *et al* 1999). Du *et al* (1998) reported a baseline saturation of 84% for a piglet head with the scalp removed, and Ma *et al* (1999) reported 78% after application of background correction. Second the StO<sub>2</sub>

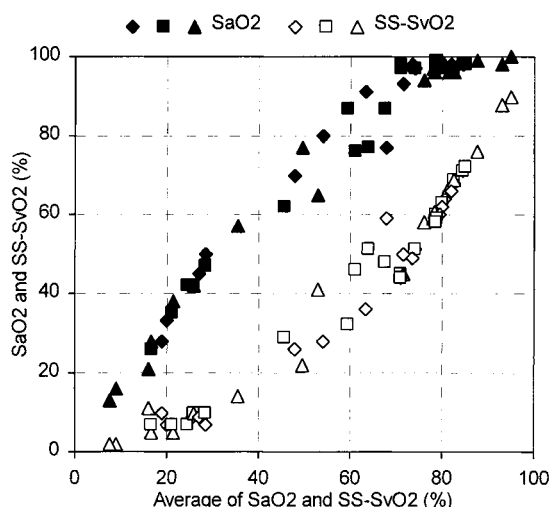


Figure 5. Correlations of  $\text{SaO}_2$  and  $\text{SS-SvO}_2$  with the average of  $\text{SaO}_2$  and  $\text{SS-SvO}_2$ .

seems to ‘under-respond’;  $\text{StO}_2$  changes less than  $\text{SS-SvO}_2$  and  $\text{SaO}_2$  during the protocol. At extreme hypoxia,  $\text{StO}_2$  is sometimes equal to (or even slightly greater than)  $\text{SaO}_2$ , and during hyperoxia,  $\text{StO}_2$  is equal to or less than  $\text{SS-SvO}_2$ . In other words, the mixture of  $\text{SaO}_2$  to  $\text{SS-SvO}_2$  that corresponds to  $\text{StO}_2$  not only changes with  $\text{FiO}_2$  but in some cases  $\text{StO}_2$  actually does not lie between  $\text{SS-SvO}_2$  and  $\text{SaO}_2$ . While one might expect  $\text{StO}_2$  to become closer to  $\text{SaO}_2$  during vascular dilation, and closer to  $\text{SvO}_2$  during vascular contraction, the observed changes appear excessive. Also, the measured [total-Hb] does not indicate significant vascular contraction during hyperoxygenation, only dilation during hypoxoxygenation.

#### 4.3. Potential sources of systematic error which may contribute to the apparent anomalies

The FDMD method applied in this study is based on the simplifying assumption that tissues can be treated as a flat macroscopically homogeneous medium. However, the piglet head is neither flat nor homogeneous. The piglet’s head is both curved and layered, with several layers between the optical probe and the brain (scalp, cranium, dura mater etc). Therefore, an error may arise due to the mismatch between the sample’s actual morphology and the simple model used. For purposes of this discussion, we can enumerate three categories of errors. Errors caused by the layered nature of the sample, errors caused by sample curvature, and absorption–scattering ‘cross-talk’.

The FDMD method is less affected by superficial layers than are single-distance methods. While analytical solutions to the two-layered model have been reported (Kienle *et al* 1998a, b), studies using the FDMD method with layered optical phantoms have demonstrated that a superficial layer 4 mm thick (or thinner) will have only a small influence on the accuracy of the measured optical properties of an underlying thick layer (Franceschini *et al* 1988). For the piglets used, the thickness of the scalp was about 2 mm and that of the cranium was about 2 mm, as measured during the dissection of several similarly sized piglets in an earlier study (Fantini *et al* 1999). Therefore, we do not believe that the anomalies described here are due predominantly to the model’s failure to account for the layered nature of the sample.

The effect of sample curvature on the FDMD method has been studied by Cerussi *et al* (1996). In that work it was found that the effect of curvature in the direction perpendicular

to the source–detector line is minimal. By contrast, a curvature along the source–detector line leads to an underestimation of both the absorption and the reduced scattering coefficients. While the curvature of the piglet’s head may contribute to the effective background absorption found in this study, the expected error is opposite in sign and smaller than the apparent error observed in this study.

Another possible mechanism for error is a ‘cross-talk’ between the  $\mu_a$  and  $\mu'_s$  due to the simplifications (homogeneity and semi-infinite boundary conditions) made in the theory. For example, a real change in the scattering properties of the sample could cause an apparent change in the measured  $\mu_a$  that is not related to a real change in absorption. While laboratory studies using homogeneous, semi-infinite phantoms have shown very good separation of measured absorption and scattering, some ‘cross-talk’ may take place in highly inhomogeneous or geometrically irregular tissues.

There is some indirect evidence that absorption–scattering ‘cross-talk’ is not large enough to account for the results of this study. As part of an earlier study, the same methodology was used to observe changing in absorption and scattering in a piglet head during and after the sacrifice of the piglet (via potassium induced cardiac arrest) (Fantini *et al* 1999). Following sacrifice, the reduced scattering coefficient (at both wavelengths) showed a biphasic trace with an initial decrease (for about 5 min) and a subsequent increase (at a rate of about  $0.13 \text{ cm}^{-1} \text{ min}^{-1}$ ). By contrast, the absorption coefficient decreased monotonically after sacrifice, according to a temporal dynamic significantly different from the initial scattering decrease. During the scattering increase phase,  $\mu'_s$  had increased by about  $0.5\text{--}1.0 \text{ cm}^{-1}$ , while  $\mu_a$  was almost constant (it decreased by less than  $0.002 \text{ cm}^{-1}$ ). This suggests that large changes in scattering can occur without causing a significant change in the measured absorption.

In the present work, large changes in measured  $\mu'_s$  generally coincide with changes in measured  $\mu_a$ . In figure 2, it can be seen that during each periods of very low  $\text{FiO}_2$  (10% and 5%) there was an increase in the measured  $\mu'_s$  accompanied by increases in measured  $\mu_a$  at both wavelengths (758 nm and 830 nm). This observation may suggest absorption–scattering ‘cross-talk’. However, changes in the scattering properties are not unexpected during periods of increased tissue haemoglobin content, because the increased number of blood cells and the changes in the shape of the blood vessels (arteriole dilation) should cause changes in the scattering properties of the tissue. When  $\text{FiO}_2$  was increased following the periods of low  $\text{FiO}_2$ , both  $\mu_a$  and  $\mu'_s$  returned to near baseline values. During the recovery period, the  $\mu'_s$  curves follow the total haemoglobin concentration curve more closely than the  $\mu_a$  curves. This difference is most clear for the 830 nm curves. While some amount of absorption–scattering ‘cross-talk’ may occur, we cannot say that it is large enough (alone) to cause the apparent anomalies outlined above. However, the possibility cannot be ruled out with certainty.

Another potential source of an apparent disagreement between the  $\text{SaO}_2$  and  $\text{SS-SvO}_2$  and NIR measured  $\text{StO}_2$ , is that  $\text{StO}_2$  is a locally measured value, whereas  $\text{SaO}_2$  is a global value and  $\text{SS-SvO}_2$  represents the ‘average’ venous saturation for the brain.  $\text{SS-SvO}_2$  may not be representative of the ‘local’  $\text{SvO}_2$  in the volume probed by the tissue oximeter. Most importantly, it may be possible that during hyperoxia  $\text{SS-SvO}_2$  is higher than  $\text{SvO}_2$  in the volume probed by NIRS. Perhaps the fraction of blood in the sagittal-sinus vein that passed through the probed volume is reduced during hyperoxia, when arterial flow might be partially redirected to some less sensitive part of the brain. However, no large coincident changes in blood concentration or scattering were observed coincident with hyperoxia. In any case, the difference between  $\text{SS-SvO}_2$  and local  $\text{SvO}_2$  can never explain why  $\text{StO}_2$  is equal to (or in some cases, larger than)  $\text{SaO}_2$  under extreme hypoxia. Also, the  $\text{StO}_2$  values during hyperoxia seem



consistent with the trend seen in the other data; they fit the ‘best fit’ line in figure 4. Finally, a possible explanation of these anomalies is that the tissue has a much larger background than that due to the water alone. Under-response in  $\text{StO}_2$  would result from a larger than expected background absorption.

#### 4.4. Results using empirically determined background absorption values

Applying the method for estimating background absorption described by Ma *et al* (1999) (as outlined above), the average background absorptions calculated for piglets 2–5 were  $0.08 \text{ cm}^{-1}$  at 758 nm and  $0.06 \text{ cm}^{-1}$  at 830 nm with a standard deviation of  $0.01 \text{ cm}^{-1}$  for both wavelengths. (After the application of these background corrections, the average [total-Hb] was reduced to 0.043 mM compared with 0.063 mM with the ‘water-only’ background assumption.) By contrast, 80% water would produce a background absorption of only  $0.021 \text{ cm}^{-1}$  and  $0.025 \text{ cm}^{-1}$  respectively, which represents the opposite wavelength dependence. The wavelength dependence of the average background absorption was similar (in trend) to the absorption spectrum of deoxyhaemoglobin. However, the ratio of the deoxyhaemoglobin extinction coefficients at 758 nm to 830 nm is 2.2:1, but the ratio of the average background absorption at the two wavelengths is only 1.3:1. The wavelength dependence of the average background was similar to the wavelength dependence of the measured  $\mu'_s$ . This observation may be indicative of some absorption–scattering ‘cross talk’ (as discussed in section 4.3 above). For the data measured in the individual piglets, there did not seem to be any trend between the magnitude of  $\mu'_s$ ,  $\mu_a$  or [total-Hb] and the magnitude of the effective background absorption. More data (especially more wavelengths) would be required to make conclusions concerning the significance of the wavelength dependence of the absorption background values determined using this method.

The last two bar types in figure 3 summarize the results after corrections for estimated backgrounds. The second to last bar type represents the results when the background values for each individual piglet were applied. The last bar shows the result when the average background values were applied. The fact that the resulting  $\text{StO}_2$  values lie neatly between  $\text{SaO}_2$  and  $\text{SvO}_2$  at 27% and 10%  $\text{FiO}_2$  is not significant, since an initial mixture of 50%  $\text{SaO}_2$  and 50%  $\text{SvO}_2$  was imposed at the initial instances of these  $\text{FiO}_2$  levels. However, the fact that the resulting  $\text{StO}_2$  values no longer seem to under-respond compared with changes in  $\text{SaO}_2$  and  $\text{SvO}_2$ , and the fact that  $\text{StO}_2$  is always between  $\text{SS-SvO}_2$  and  $\text{SaO}_2$ , does confirm that background absorption alone could ‘correct’ for the anomalies described above.

Figure 6 shows the time traces of  $\text{StO}_2$  during the three  $\text{FiO}_2$  cycles for piglet 3, using all three background values; water only background, individually empirically determined background, and average empirically determined background. It appears that the use of the average background values is sufficient at every  $\text{FiO}_2$  level except 5%. Inaccuracy limited to very low saturation levels is not as troubling as inaccuracy at higher saturation values, since the ability to precisely measure  $\text{StO}_2$  values of less than 10% (in brain tissue) is of dubious clinical value.

Figure 7 shows correlation plots similar to the one in figure 4. figure 7A is the correlation between  $\text{StO}_2$  and the average of  $\text{SvO}_2$  and  $\text{SaO}_2$  using individually determined background corrections. The calculation of the ‘best fit’ line on figure 7A did not include the points used to calculate the background absorption values, since they lie on a one-to-one correlation by definition. These points are displayed as dark circles and labelled as basis points for background correction. Figure 7B is the correlation using  $\text{StO}_2$  calculated with average background values. Most notable is the fact that the nearly linear correlation is improved in both plots, and that the slopes of both lines are nearly unity. In addition, in figure 7A the intercept of the line is very

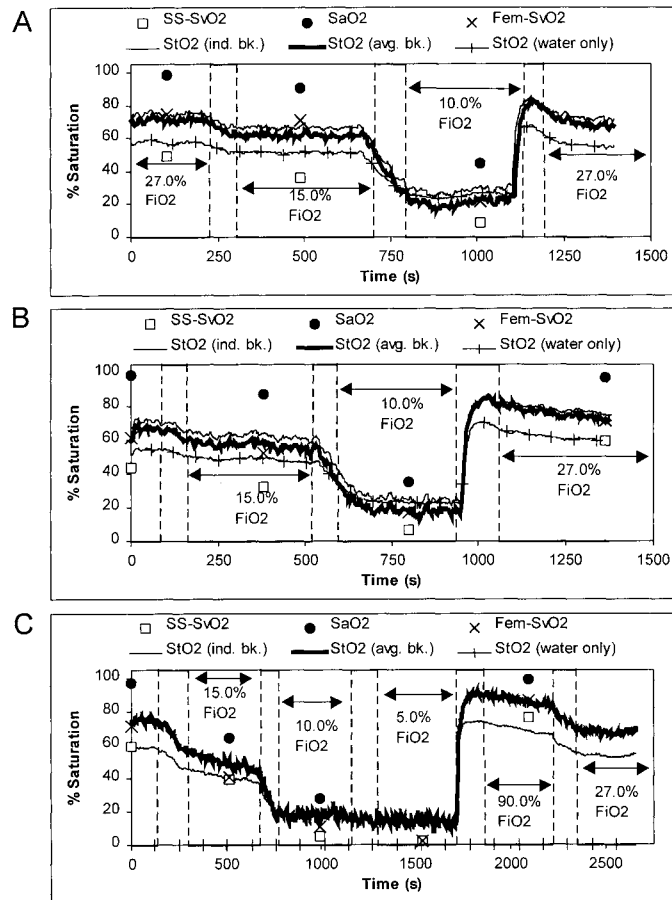


**Figure 6.** Time traces of StO<sub>2</sub> values for piglet 3 based on water-only background assumption, individually determined background values, and average background values. (A) FiO<sub>2</sub> cycle 1, (B) FiO<sub>2</sub> cycle 2, (C) FiO<sub>2</sub> cycle 3.

nearly perfect (nearly 0). Again, the perfect slopes are to be expected, since we assumed a 1:1 mixture of SaO<sub>2</sub> and SS-SaO<sub>2</sub> at 27% FiO<sub>2</sub> and 10% FiO<sub>2</sub>. However, it is significant that the corrections appear consistent at all FiO<sub>2</sub> levels, and that the average background values work very well except at very low saturation values.

Using the form  $X \times (\text{SS-SvO}_2) + [1 - X] \times \text{SaO}_2$ , where  $X$  is the fraction of SS-SvO<sub>2</sub>, figure 8 shows the fraction (or weighting) of SS-SvO<sub>2</sub> necessary to interpret StO<sub>2</sub> as a weighted average of SS-SvO<sub>2</sub> and SaO<sub>2</sub> at each FiO<sub>2</sub> level. The three background correction methods are represented. The first bar in each group illustrates the results when the absorption due to 80% water is the only background considered. The second bar type represents the results using individually determined background corrections, and the last bar type represents the results when the average empirical background values are applied to all piglets. The 'error-bars' represent one standard deviation. The fraction of SS-SvO<sub>2</sub> is greater than one, when the average StO<sub>2</sub> value (at the given FiO<sub>2</sub> level) is less than the average SS-SvO<sub>2</sub> value. It is clear that the water-only background assumption results in a large range of SS-SvO<sub>2</sub> fractions. The individually determined background correction method leads to a realistic range of SS-SvO<sub>2</sub>

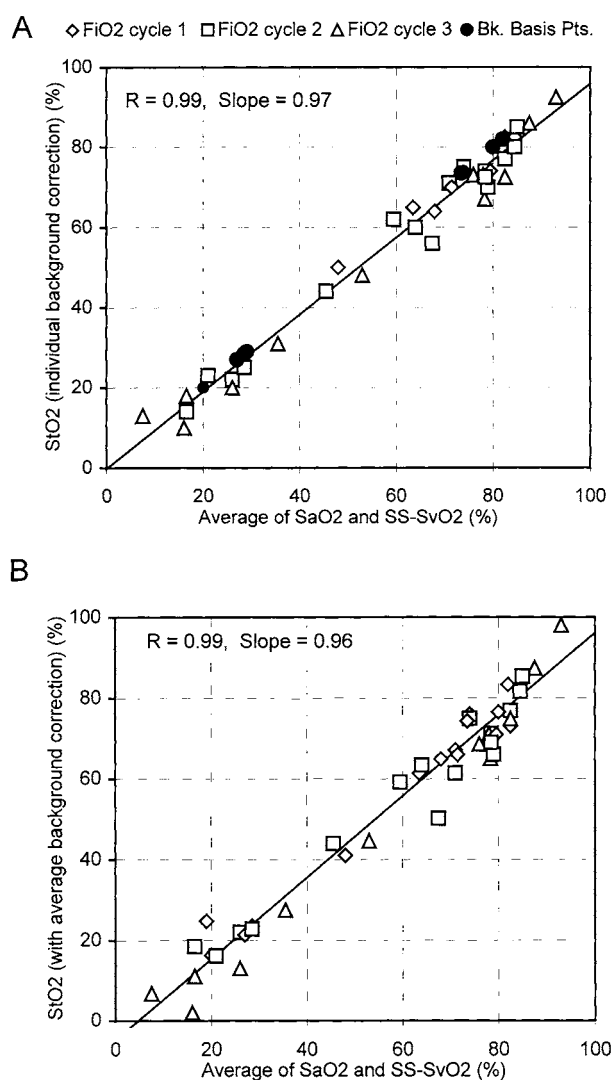


**Figure 7.** Correlation of recalculated (effective background subtracted) StO<sub>2</sub> values with average of SaO<sub>2</sub> and SS-SvO<sub>2</sub>. Lines indicate result of linear regression analysis: (A) with individually determined background values, (B) with average background values.

fractions, but there is still some trend towards lower SS-SvO<sub>2</sub> weightings at low FiO<sub>2</sub> levels, which may be due to vascular dilation. Again, application of the average background values results in similar SS-SvO<sub>2</sub> weightings at all FiO<sub>2</sub> levels except for the most extreme condition (5% O<sub>2</sub>).

It remains that the background absorption values found by this method are higher than expected. The absorption of water, and cytochrome, cannot account for this background. When modelling absorption in brain tissue, Matcher *et al* (1995) reported that a fixed baseline absorption of 0.07 cm<sup>-1</sup> had to be added to the absorption spectrum of 60 μM Hb in order to bring the absorption coefficient at 820 nm into closer agreement with the data of Van der Zee (1992). However, since we cannot identify the absorbers responsible, we must stress that

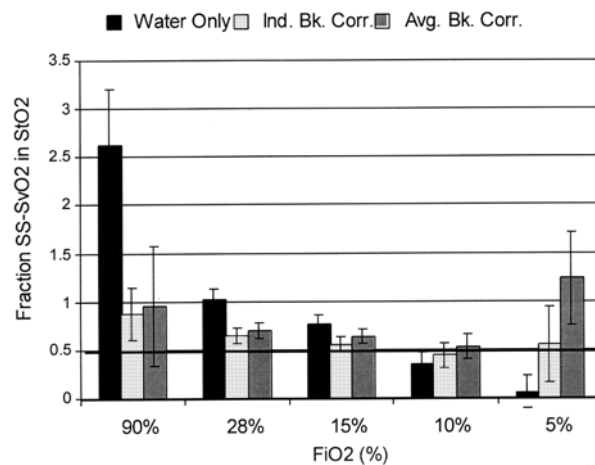


**Figure 8.** Summary of the fraction of SS-SvO<sub>2</sub> in the hypothetical mixture of SaO<sub>2</sub> and SS-SvO<sub>2</sub> that is apparently equivalent to StO<sub>2</sub>.

these values represent only an 'effective' background absorption that 'corrects' for unknown errors. These errors may be an underestimation in non-haemoglobin background, incorrect haemoglobin extinction coefficients, errors caused by the approximate nature of the FDMD method, or a combination of these and other factors.

## 5. Conclusion

A strong linear correlation was observed between FDMD-measured StO<sub>2</sub> tissue haemoglobin oxygenation and the average of SaO<sub>2</sub> and SvO<sub>2</sub> (from the superior sagittal-sinus vein) in the brains of newborn piglets using an FDMD-based instrument. Repeated measurements demonstrated a consistent relationship between StO<sub>2</sub> and both SaO<sub>2</sub> and SvO<sub>2</sub>. However, the apparent under-response of StO<sub>2</sub> seems to suggest that a larger than expected background absorption is present for the piglet head. It is also possible that discrepancies between the simple flat homogeneous model used and the curved and layered tissue sample produce a positive offset in measured absorption coefficient values. In either case, an 'effective' background resulted. Accounting for this apparent background could improve the accuracy of the FDMD method used for haemoglobin measurements on piglet heads, and may also result in improved measurements in human infants.

## References

- Araki R and Nashimoto I 1989 Multicomponent analysis of near infrared spectra of anaesthetised rat head: (I) Estimation of component spectra by principal component analysis *Adv. Exp. Med. Biol.* **248** 3–10
- Arridge S R, Cope M and Delpy D T 1992 The theoretical basis for the determination of optical pathlengths in tissue: temporal and frequency analysis *Phys. Med. Biol.* **37** 153–60
- Benaron D A, Kurth C D, Steven J, Wagerle L C, Chance B and Delivoria-Papadopoulos M 1989 Non-invasive estimation of cerebral oxygenation and oxygen consumption using phase-shift spectrophotometry *Proc. IEEE* **12** 2004–6
- Benaron D A and Stevenson D K 1993 Optical time-of-flight and absorbance imaging of biological media *Science* **259** 1463–6
- Brun N C, Moen A, Borch K, Saugstad O D and Greisen G 1997 Near-infrared monitoring of cerebral tissue oxygen saturation and blood volume in newborn piglets *Am. J. Physiol.* **273** H681–H686

- Cerussi A, Maier J, Fantini S, Franceschini M A and Gratton E 1996 The frequency-domain multi-distance method in the presence of curved boundaries *OSA Trends in Optics and Photonics on Biomedical Optical Spectroscopy and Diagnostics* vol 3, ed E Sevick-Muraca and D Benaron (Washington, DC: Optical Society of America) pp 92–7
- Chance B (ed) 1989 *Photon Migration in Tissue* (New York: Plenum)
- Chance B and Alfano R (eds) 1997 Proceedings of optical tomography and spectroscopy of tissue: theory, instrumentation, model and human studies II *Proc. SPIE* **2979**
- Chance B, Alfano R and Tromberg B (eds) 1999 Proceedings of optical tomography and spectroscopy of tissue: theory, instrumentation, model and human studies III *Proc. SPIE* **3597**
- Cope M and Delpy D T 1988 System for long-term measurement of cerebral blood and tissue oxygenation in newborn infants by near infrared transillumination *Med. Biol. Eng.* **26** 289–94
- Cope M, Van der Zee P, Essenpreis M, Arridge S R and Delpy D T 1991 Data analysis methods for near infrared spectroscopy of tissues: problems in determining the relative cytochrome aa3 concentration *Proc. SPIE* **1431** 251–63
- Du C, Andersen C and Chance B 1998 Quantitative detection in haemoglobin saturation on piglet brain by near-infrared frequency-domain spectroscopy *Proc. SPIE* **3194** 55–63
- Edwards A D, Wyatt J S, Richardson C, Potter A, Delpy D T, Cope M and Reynolds E O R 1988 Cotside measurement of cerebral blood flow in ill newborn infants by near infrared spectroscopy *Lancet* **ii** 770–1
- Fantini S, Franceschini M A, Fishkin J B, Barbieri B and Gratton E 1994b Quantitative determination of the absorption spectra of chromophores in strongly scattering media: a light-emitting-diode based technique *Appl. Opt.* **33** 5204–13
- Fantini S, Franceschini M A and Gratton E 1994a Semi-infinite geometry boundary problem for light migration in highly scattering media: a frequency domain study in the diffusion approximation *J. Opt. Soc. Am. B* **11** 2128–38
- Fantini S, Franceschini M A, Maier J S, Walker S A, Barbieri B and Gratton E 1995 Frequency-domain multichannel optical detector for non-invasive tissue spectroscopy and oximetry *Opt. Eng.* **28** 32–42
- Fantini S, Hueber D, Franceschini M A, Gratton E, Resonfeld W, Stubblefield P G, Maulik D and Stankovic M R 1999 Non-invasive optical monitoring of the newborn piglet brain using continuous wave and frequency domain spectroscopy *Phys. Med. Biol.* **44** 1543–63
- Farrel T, Patterson M S and Wilson B 1992 A diffusion theory model of spatially resolved, steady-state diffuse reflectance for the noninvasive determination of tissue optical properties *in vivo Med. Phys.* **19** 879–88
- Fishkin J B and Gratton E 1993 Propagation of photon-density waves in strongly scattering media containing an absorption semi-infinite plane bounded by a straight edge *J. Opt. Soc. Am. A* **10** 127–40
- Franceschini M A, Fantini S and Gratton E 1998 Influence of a superficial layer in the quantitative spectroscopic study of strongly scattering media *Appl. Opt.* **37** 7447–58
- Franceschini M A, Wallace D, Barbieri B, Fantini S, Mantulin W W, Pratesi S, Donzelli G P, Gratton E 1997 Optical study of the skeletal muscle during exercise with a second generation frequency-domain tissue-oximeter *Proc. SPIE* **2979** 807–14
- Jöbsis F F 1989 Non-invasive infrared monitoring of cerebral myocardial oxygen sufficiency and circulatory parameters *Science* **198** 1264–7
- Karagiannes J L, Zhang Z, Grossweiner B and Grossweiner L I 1989 Applications of the 1-D diffusion approximation to the optics of tissues and tissue phantoms *Appl. Opt.* **28** 2311–17
- Kienle A, Glanzmann T, Wagnières G and van der Bergh H 1998b Investigation of two-layered turbid media with time-resolved reflectance *Appl. Opt.* **37** 6852–62
- Kienle A, Patterson M S, Dögnitz N, Bays R, Wagnières G and van der Bergh H 1998a Noninvasive determination of the optical properties of two-layered turbid media *Appl. Opt.* **37** 779–91
- Liu H, Boas D, Zhang Y, Yodh A and Chance B 1995a A simplified approach to characterize optical properties and blood oxygenation in tissue using continuous near infrared light *Proc. SPIE* **2389** 496–502
- Liu H, Hielscher A H, Beauvoit B, Wang L, Jacques S L, Tittel F K and Chance B 1995b Near Infrared spectroscopy of a heterogeneous, turbid system containing distributed absorber *Proc. SPIE* **2326** 164–72
- Ma H Y, Xu Q, Ballesteros J R, Ntziachristos V, Zhang Q and Chance B 1999 Quantitative study of hypoxia stress in piglet brain by IQ phase modulation oximetry *Proc. SPIE* **3597** 642–9
- Matcher S J, Elwell C E, Cooper C E, Cope M and Delpy D T 1995 Performance comparison of several published tissue near-infrared spectroscopy algorithms *Anal. Biochem.* **227** 54–68
- Miwa M, Ueda Y and Chance B 1995 Development of time resolved spectroscopy system for quantitative non-invasive tissue measurement *Proc. SPIE* **2336** 142–9
- Patterson M S, Chance B and Wilson B C 1989 Time resolved reflectance and transmittance for the noninvasive measurement of tissue optical properties *Appl. Opt.* **28** 2331–6
- Sevick E M, Chance B, Leigh J, Nioka S and Maris M 1991 Quantitation of time- and frequency-resolved optical spectra for the determination of tissue oxygenation *Anal. Biochem.* **195** 330–51

- Stankovic M R, Fujii A, Maulik D, Boas D, Kirby D and Stubblefield P G 1998 Optical monitoring of cerebral haemodynamics and oxygenation in the neonatal piglet *J. Matern. Fetal Invest.* **8** 71–8
- Stankovic M R, Maulik D, Rosenfeld W, Stubblefield P G, Kofinas A D, Drexler S, Nair R, Franceschini M A, Hueber D, Gratton E and Fantini S 1999 Real-time optical imaging of experimental brain ischemia and haemorrhage in neonatal piglets *J. Perinatal Med.* **27** 279–86
- Swain D P and Pittman R N 1989 Oxygen exchange in the microcirculation of hamster retractor muscle *Am. J. Physiol. Soc.* **255** H247–H255
- Tromberg B J, Svaasand L O, Tsay T T, Haskell R C and Berns W M 1991 Optical property measurement in turbid media using frequency-domain photon migration *Proc. SPIE* **1525** 52–8
- Van der Zee P 1992 Measurement and modelling of the optical properties of human tissue in the near infrared *Thesis* Department of Medical Physics and Bioengineering, University College London pp 246–91
- Wahr J A *et al* 1996 Near-infrared spectroscopy: theory and applications *J. Cardiothoracic. Vascular Anesthesia* **3** 406–18
- Wallace D, Michener B, Choudhury D, Levi M and Fennelly P 1999 Results of a 95-subject human clinical trial for the diagnosis of peripheral vascular disease using a near-infrared frequency domain haemoglobin spectrometer *Proc. SPIE* **3597** 300–16
- Wray S, Cope M, Delpy D T, Wyatt J and Reynolds R 1988 Characterization of the near infrared absorption spectra of cytochrome aa<sub>3</sub> and haemoglobin for the noninvasive monitoring of cerebral oxygenation *Biochem. Biophys. Acta* **933** 184–92
- Yamashita Y, Oda M, Naruse H and Tamura M 1996 *In vivo* measurement of reduced scattering coefficient and absorption coefficient of living using tissue time-resolved spectroscopy *OSA Trends in Optics and Photonics in Advances on Optical Imaging and Photon Migration* vol 2 (Washington, DC: Optical Society of America) pp 387–90